

Investigation of ${}^6\text{Li} + {}^{64}\text{Ni}$ fusion at near-barrier energiesMd. Moin Shaikh,¹ Subinit Roy,^{1,*} S. Rajbanshi,¹ M. K. Pradhan,¹ A. Mukherjee,¹ P. Basu,¹ S. Pal,²
V. Nanal,² R. G. Pillay,² and A. Shrivastava³¹*Saha Institute of Nuclear Physics, 1/AF, Bidhan Nagar, Kolkata 700 064, India*²*Department of Nuclear and Atomic Physics, Tata Institute of Fundamental Research, Mumbai 400 005, India*³*Nuclear Physics Division, Bhabha Atomic Research Centre, Mumbai 400 085, India*

(Received 25 June 2014; published 21 August 2014)

The total fusion (TF) excitation function for a ${}^6\text{Li}$ projectile with a ${}^{64}\text{Ni}$ target has been measured using the online characteristic γ ray detection method at energies around the Coulomb barrier. The complete fusion (CF) excitation function for the system is subsequently estimated from the dominating neutron evaporation channels with the help of statistical model predictions. The CF cross sections exhibit a suppression of about 13% compared to the one-dimensional barrier penetration model (1DBPM) at above-barrier energies, but no suppression is observed for TF cross sections. The observation does corroborate the estimated suppression for ${}^6\text{Li}$ on ${}^{59}\text{Co}$ target, but does not corroborate the recently proposed universal suppression factor for the ${}^6\text{Li}$ projectile. The result supports the conjecture of reduced suppression of CF cross sections with decreasing target mass. At energies below the barrier, both the TF and the CF cross sections are enhanced. The observed enhancement of the CF process can be explained by channel coupling (CC), but the enhancement in TF cross sections is significantly higher than the CC predictions.

DOI: [10.1103/PhysRevC.90.024615](https://doi.org/10.1103/PhysRevC.90.024615)

PACS number(s): 25.70.Gh, 24.10.Eq, 25.60.Pj

I. INTRODUCTION

The breakup of a weakly bound projectile into its constituent clusters in the field of the target nucleus dynamically affects the fusion of the two nuclei in several ways [1,2]. Besides increasing the direct reaction cross section, it modifies the cross section of the complete fusion (CF) reaction through reaction processes such as the sequential complete fusion (SCF) of all the fragments after breakup of the projectile, a process experimentally indistinguishable from the CF process, and/or the incomplete fusion (ICF) of one of the breakup fragments of the projectile [3].

In experiments with weakly bound, stable projectiles such as ${}^6\text{Li}$ ($S_\alpha = 1.47$ MeV), ${}^7\text{Li}$ ($S_\alpha = 2.45$ MeV), and ${}^9\text{Be}$ ($S_n = 1.67$ MeV) on heavy targets [4–9], the two fusion processes, CF and ICF, can be clearly identified. In the case of heavy targets, the residues produced by the two reaction mechanisms are different, as the evaporation of charged particles from compound nucleus is hindered due to the higher Coulomb barrier associated with the process. The observations suggest that the CF cross sections at above-barrier energies are suppressed in comparison with the predictions of the one-dimensional barrier penetration model (1DBPM). It was shown that the observed suppression is almost accounted for by the ICF cross sections in the above-barrier energy region [4], and the total fusion, $\text{TF} = \text{CF} + \text{ICF}$, cross sections are unaffected by the breakup of the projectile. It has been subsequently established that the magnitude of the suppression is a function of the breakup threshold of the projectile [10]. With decreasing mass of the target, it becomes experimentally difficult to isolate the residues of the ICF channels, as in most cases they are indistinguishable from the residues of the CF

channels. The measurement, therefore, yields only the TF cross section. Consequently, to infer the magnitude of suppression of the CF cross section at above-barrier energies is quite difficult in the case of low mass targets. In the attempt to estimate the effect of breakup of the projectile on the fusion reaction involving lower mass targets, two different scenarios have evolved. In one, the suppression of CF cross sections at above the barrier energies is said to diminish [4,7,11] with decreasing charge of the target, suggesting a dominant role of the Coulomb interaction in the process. The other picture evolved from a recent work of Kumawat *et al.* [12] where the authors, through an indirect method of estimation of CF cross section, proposed the existence of a universal suppression factor of approximately 30% for CF of a ${}^6\text{Li}$ projectile with different targets at above barrier energies. The authors concluded that nuclear interaction plays the more dominant role over the Coulomb interaction in producing breakup at higher energies, and hence the suppression of CF is independent of target charge. However, an exception was observed for the ${}^6\text{Li} + {}^{59}\text{Co}$ system with a $\sim 15\%$ suppression of CF cross section.

In the below-barrier energy region, both the TF and the CF excitation functions of weakly bound projectiles on heavy targets, in general, show enhancement compared to the 1DBPM predictions [13]. On the other hand, the situation for fusion of these projectiles with medium mass targets is unclear [14]. A comparison of the measured TF cross sections for ${}^{6,7}\text{Li}$ isotopes with ${}^{59}\text{Co}$ [15] and ${}^{64}\text{Zn}$ [16] targets suggests larger enhancement for ${}^6\text{Li}$ relative to ${}^7\text{Li}$ at sub-barrier energies. However, it has been pointed out in Ref. [16] through a careful analysis of the data that the enhancement of TF cross sections below the barrier is due to the contributions from ICF or direct cluster transfer (DCT) and/or single-particle transfer reactions. The question that automatically arises is how these processes influence the CF cross sections at low energies for medium mass targets. The answer depends primarily on the

*subinit.roy@saha.ac.in

experimental determination of the CF component of measured TF cross sections in the below-barrier energy regime. In this context, we present measurement of the fusion excitation function for a ${}^6\text{Li}$ projectile on a ${}^{64}\text{Ni}$ target. The nucleus ${}^{64}\text{Ni}$ is the heaviest of the stable Ni isotopes, with eight valence neutrons over an $N = 28$ closed subshell. With six additional neutrons compared to the most stable isotope ${}^{58}\text{Ni}$ ($N/Z = 1.07$), the compound nucleus (CN) formed in the fusion of ${}^6\text{Li}$ with ${}^{64}\text{Ni}$ ($N/Z = 1.28$) decays predominantly through $2n$ and $3n$ channels, which are pure CF decay channels. One of the primary goals of the present work is to estimate the CF cross sections from these dominant neutron evaporation channels and compare the same with the measured TF cross sections. Subsequent analysis with the derived CF cross section data addresses the question of suppression of CF cross sections at above-barrier energies for medium or lower mass targets, and also helps us to understand the natures of enhancement in the TF and CF cross sections at below the Coulomb barrier energies.

II. EXPERIMENTAL DETAILS

The experiment was carried out at the Pelletron Facility in Mumbai, India. A self-supporting $\sim 99\%$ enriched metallic ${}^{64}\text{Ni}$ target of thickness $507 \mu\text{g}/\text{cm}^2$, procured from Oak Ridge National Laboratory, USA, was used for the present experiment. The target thickness was verified with the α -energy loss method using a three-line α source (${}^{239}\text{Pu}$, ${}^{241}\text{Am}$, and ${}^{244}\text{Cm}$) and the estimated uncertainty was about 2%. The target was bombarded with ${}^6\text{Li}$ beam of energies from 11 to 28 MeV in small steps. The beam current was varied from 1 to 4 p nA, keeping the acquisition dead time within a reasonable limit of 6% to 7%. After each energy run, the background spectrum was recorded without the beam on the target. Background data was also collected with beam passing through a blank tantalum frame at the target position after each energy run. Fusion cross sections were measured from the yields of the online characteristic γ rays emitted from the evaporation residues of the compound nucleus [17]. Two high-purity germanium (HPGe) detectors were placed at 45° and 125° with respect to the beam direction to detect the γ rays. The detector resolutions were 2.8 and 2.3 keV respectively for the 1408 keV γ line of a ${}^{152}\text{Eu}$ radioactive source. Data for absolute efficiency was taken by placing calibrated radioactive sources of ${}^{152}\text{Eu}$ and ${}^{133}\text{Ba}$ at the target position before and after the experiment. The estimated error in efficiency is about 3%, which includes the uncertainty in the radioactive source strengths. A Si surface barrier detector was positioned at 30° for the verification of the target thickness. The beam current was measured with a 1-metre-long Faraday cup. The computer automated measurement and control (CAMAC) based multiparameter acquisition system LAMPS [18] was used to record the data and to perform the offline analysis. The total uncertainty in the measurement of cross sections came from the systematic errors in the target thickness and from the estimation of number of the beam particles as well as the statistical errors associated with the yields of the γ rays. A part of the data was presented at the conference FUSION14 [19]. A representative characteristic γ spectrum for ${}^6\text{Li}+{}^{64}\text{Ni}$ fusion at $E_{\text{lab}} = 28$ MeV is shown in Fig. 1. At 26 MeV energy of

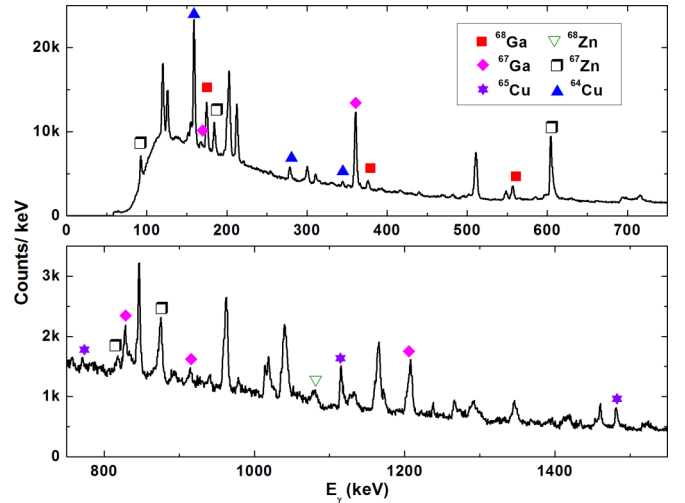


FIG. 1. (Color online) Representative γ spectrum for ${}^6\text{Li}+{}^{64}\text{Ni}$ fusion at $E_{\text{lab}} = 28$ MeV. Some of the characteristic γ transitions of the residues are marked.

the ${}^6\text{Li}$ beam, a separate run was taken using a fresh ${}^{64}\text{Ni}$ target of the same thickness along with a $4 \text{ mg}/\text{cm}^2$ thick Au catcher foil mounted behind it. The residues coming out from the target were stopped in the catcher foil. The Au foil was subsequently taken out of the chamber and placed before a x-ray detector in an of-line data acquisition arrangement. Delayed x rays from electron capture by ${}^{68}\text{Ga}$ ($T_{1/2} = 67.7$ min) and ${}^{67}\text{Ga}$ ($T_{1/2} = 2.23$ days) were recorded. The residue ${}^{68}\text{Ga}$ decays to the ground state of ${}^{68}\text{Zn}$ with a branching fraction of 97% [20]. The efficiency of the X-ray detector was determined with a standard ${}^{241}\text{Am}$ X-ray source. The energies, relative intensities and fluorescence yields of relevant K x-rays were taken from Ref. [21]. The population of ${}^{68}\text{Ga}$ coming only from CF reaction, including the contribution of direct feeding to the ground state, was determined from the offline data.

III. ANALYSIS AND RESULTS

The compound nucleus ${}^{70}\text{Ga}$ is formed in the collision of ${}^6\text{Li}$ and ${}^{64}\text{Ni}$. A statistical model calculation predicts that it decays predominantly through $2n$ and $3n$ evaporation channels, a fact that is also verified from the present experiment. Along with the pn evaporation channel, these neutron evaporation channels are associated with a purely complete fusion process. The characteristic γ rays feeding directly the ground states of the residues ${}^{68}\text{Ga}$ and ${}^{67}\text{Ga}$, identified and used in the calculation, were given in Table I. The other observed channels were pn , $p2n/dn$, αn , and $\alpha 2n$ forming residues ${}^{68}\text{Zn}$, ${}^{67}\text{Zn}$, ${}^{65}\text{Cu}$, and ${}^{64}\text{Cu}$ respectively. The residues from dn , αn , and $\alpha 2n$ decay channels can also be produced by the α -ICF and d -ICF and/or the DCT mechanisms. Each evaporation residue channel cross section ($\sigma_{\text{chn}}^{\text{exp}}$) was obtained by summing over the measured cross sections of the observed γ transitions to the ground state of the residue, i.e.,

$$\sigma_{\text{chn}}^{\text{exp}} = \sum_{\gamma} \frac{Y_{\gamma}}{\varepsilon_{\gamma} N_B N_T}, \quad (1)$$

TABLE I. Characteristic γ rays of ${}^{68}\text{Ga}$ and ${}^{67}\text{Ga}$ identified and used in the calculation.

Residue channel	Transition excited state (J^π) \rightarrow ground state (J^π)	E_γ (keV)
${}^{68}\text{Ga}$ ($2n$)	$2^+ \rightarrow 1^+$	175.0
	$1^+ \rightarrow 1^+$	321.0
	$2^+ \rightarrow 1^+$	374.6
	$(0,1,2)^+ \rightarrow 1^+$	555.5
	$2^+ \rightarrow 1^+$	564.5
	$2^- \rightarrow 1^+$	583.8
${}^{67}\text{Ga}$ ($3n$)	$1/2^- \rightarrow 3/2^-$	167.0
	$5/2^- \rightarrow 3/2^-$	359.1
	$3/2^- \rightarrow 3/2^-$	828.1
	$5/2^- \rightarrow 3/2^-$	910.9
	$7/2^- \rightarrow 3/2^-$	1202.3

where Y_γ is the γ -ray yield and ε_γ is the detector efficiency. N_B represents the number of beam particles and N_T the number of target particles per unit area. Finally, the fusion cross section was determined by the sum over cross sections of all the residue channels observed, $\sigma_{\text{fus}}^{\text{exp}} = \sum \sigma_{\text{chn}}^{\text{exp}}$. The measured individual residue cross sections along with $\sigma_{\text{fus}}^{\text{exp}}$ are plotted in Fig. 2 as a function of incident energy in the center-of-mass frame. The measured cross section $\sigma_{\text{fus}}^{\text{exp}}$ represents the cross section for the TF=CF+ICF (and/or DCT) process. It is to be mentioned that, in equating the measured cross section $\sigma_{\text{fus}}^{\text{exp}}$ to the TF cross section, the contribution of direct population of the ground states of the residues has been neglected for this system. An estimate of the contribution of direct ground state feeding can be obtained from the offline measurement of delayed x rays following electron capture by ${}^{68}\text{Ga}$ ($T_{1/2} = 67.7$ m). The measurement carried out at $E_{\text{lab}} = 26$ MeV provided the total

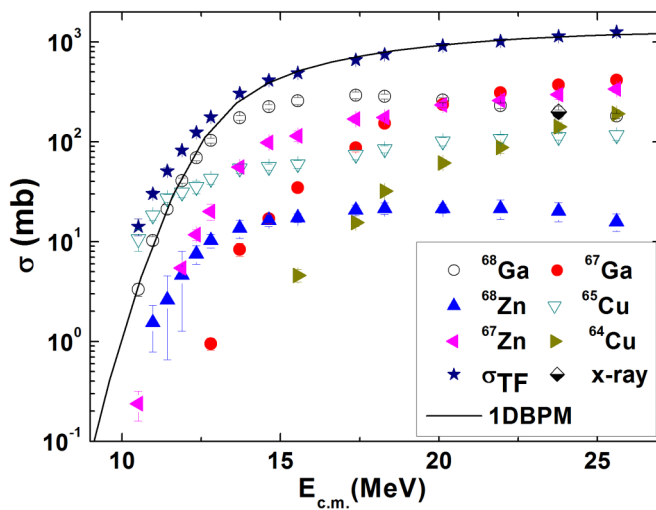


FIG. 2. (Color online) The measured excitation functions of individual residue channels are shown along with the experimental TF excitation function for the system ${}^6\text{Li} + {}^{64}\text{Ni}$. The solid line represents the 1DBPM prediction for fusion. The cross section of the residue ${}^{68}\text{Ga}$ for $E_{\text{lab}} = 26$ MeV from off-line x-ray measurement is shown by a half-filled diamond at the corresponding relative energy value.

cross section for population of the ${}^{68}\text{Ga}$ residue including the direct ground state population component, shown by a half-filled diamond in Fig. 2. Excellent matching of the cross sections measured by online and offline techniques supports the assumption [17,22,23] that the correction for direct ground state feeding is negligibly small in this mass region. The comparison also indicates that the fraction of undetected gamma transitions is negligibly small for this channel. The 1DBPM prediction for the fusion excitation function is also shown in Fig. 2 with a solid line. The calculation was performed with the code CCFULL [24], using the Akyüz-Winther potential [25] in Woods-Saxon form. The potential parameters used were strength $V_0 = 41.47$ MeV, radius parameter $r_0 = 1.17$ fm, and diffuseness $a_0 = 0.60$ fm. The resultant uncoupled barrier height V_B , barrier radius R_B , and barrier width $\hbar\omega$ obtained are 12.41 MeV, 9.1 fm, and 3.9 MeV respectively. To look for the sensitivity of the calculated 1DBPM curve on the variation of the parameters of the Woods-Saxon potential form, we chose a diffuseness parameter $a_0 = 0.75$ fm. The choice is guided by the best-fit values of the parameters fitting the elastic scattering angular distributions over the same energy region [26]. In CCFULL, the 1DBPM calculation with larger diffuseness requires deeper potential strength to avoid oscillations in transmission coefficients of high partial waves affecting the fusion cross sections at higher energies [10,27]. The parameters V_0 and r_0 were then varied to reproduce the barrier strength and radius values within 1% of the previous values. However, the width was found to be lower by about 10%. The resultant fusion excitation function differs from that with the Akyüz-Winther potential by less than 4% in the high energy region. A detailed discussion regarding the choice of the ion-ion potential to describe the fusion data can be found in Ref. [2]. Since the primary aim of the work is not to fit the data with 1DBPM, in the subsequent systematic analysis 1DBPM will refer to the uncoupled calculation using CCFULL with only the Akyüz-Winther potential, which was used as a standard ion-ion potential for other systems as well [4–8,10]. It is to be noticed that the 1DBPM prediction reproduces the measured TF cross section in the above-barrier energy range but underpredicts the measured values in the below-barrier region.

In order to estimate the CF cross section, we used the statistical model code PACE4 [28]. First, the statistical model estimates of the two most dominating neutron evaporation channels, $2n$ and $3n$, were summed to get $\sigma_{2n+3n}^{\text{stat}}$. The summed cross section of $2n$ and $3n$ decay channels contribute about 78% to 48% of the model predicted fusion cross section, taken to be the CF cross section over the energy range of 11.5 to 28 MeV. Subsequently, the ratio of $\sigma_{2n+3n}^{\text{stat}}$ to the model prediction of CF cross section, $\sigma_{CF}^{\text{stat}}$, was determined. A comparison of $\sigma_{2n+3n}^{\text{stat}}$ with the measured $\sigma_{2n+3n}^{\text{exp}}$ is shown in Fig. 3. Reasonably good agreement is observed over the whole energy range that strengthens the assumption that the contribution, if any, of the gamma transitions that might not have been detected is not significant. The CF cross section, σ_{CF}^{2n+3n} , considering only the $2n$ and $3n$ evaporation channels was then derived using the relation

$$\sigma_{CF}^{2n+3n} = \sigma_{2n+3n}^{\text{exp}} \frac{\sigma_{CF}^{\text{stat}}}{\sigma_{2n+3n}^{\text{stat}}}. \quad (2)$$

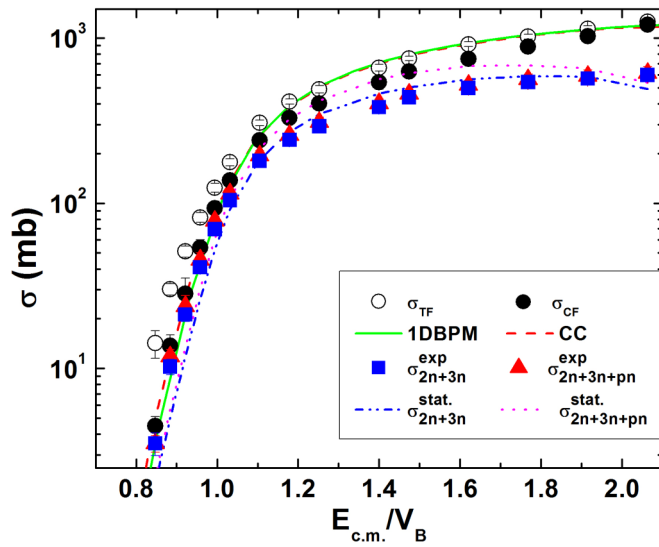


FIG. 3. (Color online) The measured TF (solid star), derived CF (solid bullet), experimental $(2n+3n)$ (solid rectangle), and $(2n+3n+pn)$ (solid triangle) excitation functions for ${}^6\text{Li}+{}^{64}\text{Ni}$. The 1DBPM and CC predictions are shown by solid and dashed lines. The PACE predictions for $\sigma_{2n+3n}^{\text{stat}}$ and $\sigma_{2n+3n+pn}^{\text{stat}}$ are shown with dot-dot-dashed and dotted lines respectively. See the text for details.

Since pn is also a decay channel originating purely from the CF process, we performed the same calculation considering the $2n$, $3n$, and pn cross sections. The $2n+3n+pn$ cross section forms about 82% to 53% of the CF cross section in the explored energy range. The resulting $\sigma_{CF}^{2n+3n+pn}$ is somewhat lower than that derived considering the $2n$ and $3n$ channels, as shown in Fig. 4. This is possibly because of the overprediction of $\sigma_{2n+3n+pn}^{\text{stat}}$ compared to $\sigma_{2n+3n+pn}^{\text{exp}}$, as is evident from Fig. 3, coming from the overprediction by the statistical model estimate of the pn channel cross section. Although the two

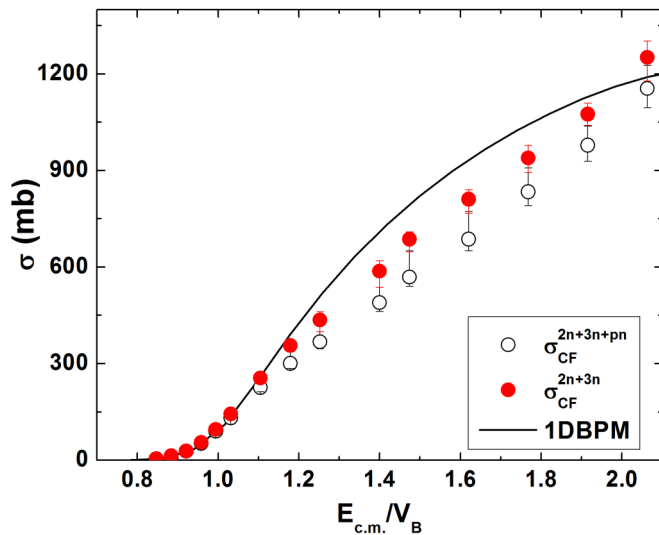


FIG. 4. (Color online) An expanded plot in linear scale, showing the comparison of σ_{CF}^{2n+3n} and $\sigma_{CF}^{2n+3n+pn}$ with the corresponding 1DBPM prediction as a function of the ratio $E_{c.m.}/V_B$.

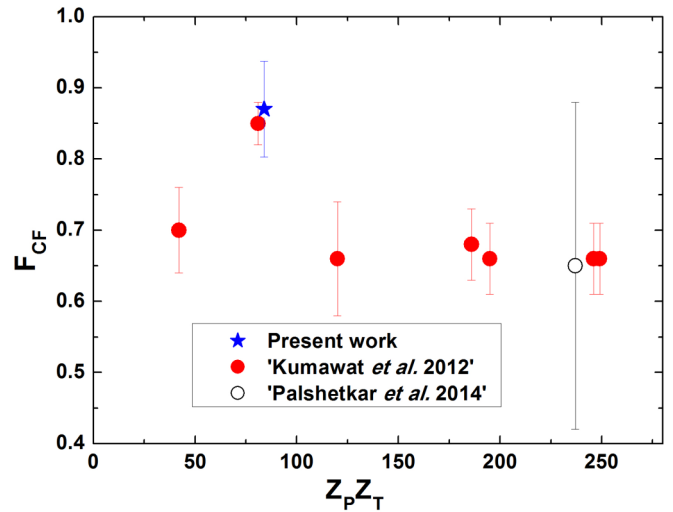


FIG. 5. (Color online) The suppression factor of σ_{CF} with respect to the 1DBPM prediction (F_{CF}) in the above-barrier energy regime is plotted as a function of projectile-target charge product, $Z_p Z_T$. The data points represented by the solid circle are taken from Kumawat *et al.* [12] and the open circle from Palshetkar *et al.* [9].

cross sections, σ_{CF}^{2n+3n} and $\sigma_{CF}^{2n+3n+pn}$, are very similar in the below-barrier region, they differ in the above-barrier region. Hence, in Fig. 3, the derived CF cross section, σ_{CF} (solid circle), is taken to be the average of σ_{CF}^{2n+3n} and $\sigma_{CF}^{2n+3n+pn}$ values. Clearly the suppression factor is different for the two cases. When compared with the prediction of 1DBPM, the average suppression factor for σ_{CF}^{2n+3n} was found to be $0.91^{+0.05}_{-0.60}$ while that for $\sigma_{CF}^{2n+3n+pn}$ was about $0.80^{+0.10}_{-0.04}$. The error limits were estimated considering the uncertainties in fitting as well as the statistical and systematic uncertainties in the data. The error-weighted final CF suppression factor for ${}^6\text{Li}+{}^{64}\text{Ni}$ was found to be 0.87 with an uncertainty of ± 0.07 . In Fig. 5, the CF suppression factor ($F_{CF} = \sigma_{CF}^{\text{exp}}/\sigma_{1DBPM}$) for ${}^6\text{Li}+{}^{64}\text{Ni}$, along with that for other projectile target combinations taken from Ref. [12], has been plotted as function of projectile target charge product $Z_p Z_T$. The resultant suppression factor of about 0.87 for ${}^6\text{Li}+{}^{64}\text{Ni}$ ($Z_p Z_T = 84$) is very close to the suppression factor for a CF cross section of ${}^6\text{Li}+{}^{59}\text{Co}$ ($Z_p Z_T = 81$). Thus our observation does not corroborate with the proposed “universal suppression factor” of Refs. [12]. It is to be noted that to reach the conclusion of universal suppression for ${}^6\text{Li}$, the authors of Ref. [12] ignored the data point corresponding to the ${}^6\text{Li}+{}^{59}\text{Co}$ system but emphasized the data point related to ${}^6\text{Li}+{}^{28}\text{Si}$ system with a still lower $Z_p Z_T$ value of 42. With only two data points below $Z_p Z_T = 100$, the conclusion based on only one of the points does not seem to be appropriate. The present study yields another data point in the region of $75 \leq Z_p Z_T \leq 100$. The consistency of the suppression factors for the two systems, ${}^6\text{Li}+{}^{59}\text{Co}$ and ${}^6\text{Li}+{}^{64}\text{Ni}$, estimated adopting two different techniques, reiterate the observation that the suppression of CF cross section in this mass region is around 15%. Hence the result of the present investigation strengthens the conjecture of reduced suppression of CF cross section with decreasing charge of

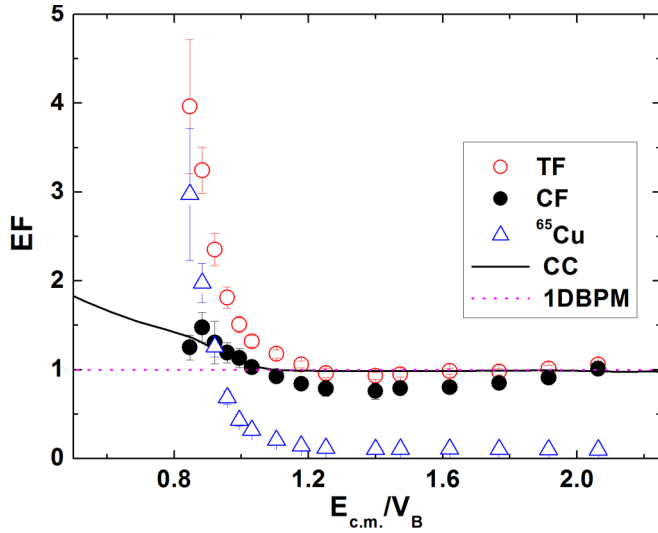


FIG. 6. (Color online) The enhancement factor of TF, CF, and CC cross sections relative to the 1DBPM cross sections plotted as a function of $E_{c.m.}/V_B$ where V_B is the height of the Coulomb barrier.

the target. However, further experiments with systems having $Z_P Z_T$ above or below the value of 80 are required to firmly establish the conclusion. The cross sections σ_{TF} and derived σ_{CF} in the below-barrier region show enhancement compared to the prediction of 1DBPM. The enhancement of σ_{TF} is significantly higher than the enhancement observed in σ_{CF} . To explore the below-barrier behavior of the cross sections, a simple coupled channel calculation with the code CCFULL was performed. The first excited state of ${}^{64}\text{Ni}$ ($J^\pi = 2^+$, $E^* = 1.345$ MeV) with deformation $\beta_2 = 0.163$ [29] and the first resonance state of ${}^6\text{Li}$ ($J^\pi = 3^+$, $E^* = 2.186$ MeV) with $B(E2) = 21.8$ e 2 fm 4 [15] were coupled. The coupled channels calculation reproduces the derived CF cross section in the below-barrier region but overpredicts the cross section values at higher energies. To amplify the degree of enhancement in CF and TF cross sections compared to the 1DBPM prediction, we plotted in Fig. 6 the enhancement factor,

$$EF = \frac{\sigma_i}{\sigma_{1DBPM}}, \quad i = \text{TF, CF, CC} \quad (3)$$

as a function of $E_{c.m.}/V_B$. The enhancement of CC cross sections describes the enhancement in CF cross section nicely, indicating that the enhancement in CF cross sections in the sub-barrier region is caused by the coupling to the inelastic excitation of the projectile and the target. Coupling to the breakup continuum is not significant at low energies for this mass region. On the other hand, the observed enhancement in TF cross sections relative to the 1DBPM calculation is much higher than the enhancements in CF or CC cross sections. Looking carefully at the below-barrier region of the excitation functions in Fig. 2, one can see that the cross sections for the residue channel ${}^{65}\text{Cu}$ becomes comparable to or even more than the most dominating $2n$ evaporation channel from the CF process in this energy regime. A plot describing the population of ${}^{65}\text{Cu}$ relative to the 1DBPM prediction over the measured energy range is also included in Fig. 6 (open triangles). It is

to be emphasized that the nucleus ${}^{65}\text{Cu}$ can be produced by reactions like d -ICF and/or DCT of d ($Q = 10.82$ MeV) as well as the one-proton stripping channel with a Q value of 3.021 MeV besides the CF process. Relatively large enhancement of ${}^{65}\text{Cu}$ production cross sections at below-barrier energies compared to the enhancement in CF cross sections indicates the domination of noncompound processes. In Fig. 6, the suppression of CF and nonsuppression of TF cross sections at above-barrier energies are clearly visible as well.

IV. SUMMARY AND CONCLUSION

To summarize, the measurement of total fusion excitation has been performed for the stable weakly bound projectile ${}^6\text{Li}$ with the medium mass target ${}^{64}\text{Ni}$ at near-barrier energies. The identification of evaporation residues and measurement of their cross sections have been done using the online characteristic γ -ray detection technique. The CF cross sections are derived from the domination of neutron evaporation channels that do not have any contributions from ICF or transfer reactions. The measured TF cross sections show a good agreement with the 1DBPM prediction in the above-barrier region. Therefore, no suppression of TF cross section is observed at above-barrier energies. The derived CF cross sections show an average suppression of 13% at higher energies and the behavior corresponds with that of target ${}^{59}\text{Co}$ in the same mass range. The consistency of the suppression of two systems justifies the conjecture that suppression of CF cross section decreases with decreasing charge of the target.

At energies below the barrier, both the TF and the CF cross sections are enhanced. While the enhancement in CF cross section can be explained by coupling the excited states of the target and the projectile, the enhancement in TF cross section is significantly larger compared to 1DBPM or CC predictions. The contribution of the residue channel ${}^{65}\text{Cu}$ in the low energy section is found to be primarily responsible for the enhancement of TF. The nucleus ${}^{65}\text{Cu}$ can be produced by d -ICF, d transfer to unbound states, one-proton stripping reactions, and also by CF processes. The analysis indicates that the production of ${}^{65}\text{Cu}$ at low energies is predominantly from processes other than the CF reaction. However, the present experiment is not designed to distinguish the reaction mechanisms producing ${}^{65}\text{Cu}$. The identification of the reaction mechanisms will be of great interest to understand the enhancement in the TF process.

ACKNOWLEDGMENTS

We sincerely thank the Pelletron staff for providing a steady and uninterrupted ${}^6\text{Li}$ beam. We would also like to thank Mr. Aditya Agnihotri, Mr. Kiran Divekar of DNAP, TIFR, and Dr. Rahul Tripathy, RCD, BARC for their support during the experiment. One of the authors, Md.M.S., would like to thank the Council of Scientific & Industrial Research, India for financial support.

- [1] L. F. Canto, P. R. S. Gomes, R. Donangelo, and M. S. Hussein, *Phys. Rep.* **424**, 1 (2006).
- [2] B. B. Back, H. Esbensen, C. L. Jiang, and K. E. Rehm, *Rev. Mod. Phys.* **86**, 317 (2014)
- [3] P. R. S. Gomes, I. Marti, M. D. Rodríguez, G. V. Marti *et al.*, *Phys. Lett. B* **601**, 20 (2004).
- [4] D. J. Hinde, M. Dasgupta, B. R. Fulton, C. R. Morton, R. J. Wooliscroft, A. C. Berriman, and K. Hagino, *Phys. Rev. Lett.* **89**, 272701 (2002).
- [5] Y. W. Wu *et al.*, *Phys. Rev. C* **68**, 044605 (2003).
- [6] M. Dasgupta *et al.*, *Phys. Rev. C* **70**, 024606 (2004).
- [7] P. K. Rath *et al.*, *Phys. Rev. C* **79**, 051601(R) (2009).
- [8] M. K. Pradhan *et al.*, *Phys. Rev. C* **83**, 064606 (2011).
- [9] C. S. Palshetkar *et al.*, *Phys. Rev. C* **89**, 024607 (2014).
- [10] A. Mukherjee *et al.*, *Phys. Lett. B* **636**, 91 (2006).
- [11] P. R. S. Gomes, R. Linares, J. Lubian, C. C. Lopes, E. N. Cardozo, B. H. F. Pereira, and I. Padron, *Phys. Rev. C* **84**, 014615 (2011).
- [12] H. Kumawat *et al.*, *Phys. Rev. C* **86**, 024607 (2012).
- [13] L. F. Canto, P. R. S. Gomes, J. Lubian, L. C. Chamon, and E. Crema, *Nucl. Phys. A* **821**, 51 (2009).
- [14] P. R. S. Gomes, J. Lubian, and L. F. Canto, *Phys. Rev. C* **79**, 027606 (2009).
- [15] C. Beck *et al.*, *Phys. Rev. C* **67**, 054602 (2003).
- [16] A. Di Pietro *et al.*, *Phys. Rev. C* **87**, 064614 (2013).
- [17] P. R. S. Gomes *et al.*, *Nucl. Instrum. Methods Phys. Res. A* **280**, 395 (1989).
- [18] Computer code LAMPS (Linux Advanced Multiparameter System), <http://www.tifr.res.in/~pell/lamps.html>.
- [19] Md. Moin Shaikh *et al.*, presented at FUSION14, Inter University Accelerator Centre, New Delhi, India, February 24–28, 2014 (unpublished), <http://www.epj-conferences.org/forthcoming>.
- [20] www.nndc.bnl.gov/in/nudat2
- [21] S. I. Salem, S. L. Panossian, and R. A. Krause, *At. Data Nucl. Data Tables* **14**, 91 (1974).
- [22] R. Liguori Neto, J. C. Acquadro, P. R. S. Gomes, A. Szanto De Toledo, C. F. Tenreiro, E. Crema, N. Carlin Filho, and M. M. Coimbra, *Nucl. Phys. A* **512**, 333 (1990).
- [23] S. B. Moraes *et al.*, *Phys. Rev. C* **61**, 064608 (2000).
- [24] K. Hagino, N. Rowley, and A. T. Kruppa, *Comput. Phys. Commun.* **123**, 143 (1999).
- [25] O. Akyüz and A. Winther, *Proceedings of the International School of Physics Enrico Fermi, Course LXXVII*, edited by R. A. Broglia, R. A. Ricci, and C. H. Dasso (North-Holland, Amsterdam, 1981), p. 492.
- [26] M. Biswas *et al.*, *Nucl. Phys. A* **802**, 67 (2008).
- [27] J. O. Newton *et al.*, *Phys. Lett. B* **586**, 219 (2004).
- [28] A. Gavron, *Phys. Rev. C* **21**, 230 (1980).
- [29] B. Pritychenko, J. Choquette, M. Horoi, B. Karamy, and B. Singh, *At. Data Nucl. Data Tables* **98**, 798 (2012).